Free energy of a ⟨110⟩ dumbbell interstitial defect in bcc Fe: Harmonic and anharmonic contributions

S. Chiesa,[1] P. M. Derlet,[2] and S. L. Dudarev[3,4]
[1]*NUM/ASQ-Materials Science and Simulation, Paul Scherrer Institute, CH-5232 Villigen PSI, Switzerland*
[2]*NUM-Condensed Matter Theory Group, Paul Scherrer Institute, CH-5232 Villigen PSI, Switzerland*
[3]*Culham Science Centre, EURATOM/UKAEA Fusion Association, Oxfordshire OX14 3DB, United Kingdom*
[4]*Department of Physics, Imperial College, Exhibition Road, London SW7 2AZ, United Kingdom*
(Received 7 April 2009; revised manuscript received 22 May 2009; published 17 June 2009)

The stability of interstitial defect and dislocation structures in bcc Fe as a function of temperature is believed to play a crucial role in determining defect evolution under irradiation conditions. The vibrational properties of defects constitute one contribution to the corresponding energetics and much work has been done within the harmonic approximation to determine the vibrational formation free energy and formation entropy of such defects. Defects can however exhibit strong local strain fields that break the cubic symmetry of the bcc lattice leading to large anharmonicities and a breakdown of the harmonic approximation as an accurate means to calculate vibrational thermodynamic quantities. Moreover, if defect diffusion is active at a time scale comparable to an atomic vibration, strong anharmonicities will always be present at any finite temperature. The current work investigates the vibrational free energy and entropy of the ⟨110⟩ self-interstitial dumbbell defect in bcc Fe using both harmonic and anharmonic free-energy calculation methods for a range of modern empirical potentials. It is found that depending on the empirical potential and for temperatures where diffusion is limited, the harmonic approximation is justified especially for empirical potentials that have been fitted to third-order elastic constants. The unique applicability range of such calculations for bcc Fe is also discussed given that with rising temperature spin fluctuations become increasingly important ultimately leading to a softening of the 110 shear modulus and to the α-bcc/γ-bcc structural phase transformation.

DOI: 10.1103/PhysRevB.79.214109 PACS number(s): 61.72.jj, 63.20.Ry, 65.40.gd

I. INTRODUCTION

In recent years there has been considerable activity within the radiation damage community to develop reliable and transferable empirical potentials for bcc Fe. This has been partly made possible by the availability of *ab initio*-calculated interstitial defect energies where, unique to bcc Fe, it is the ⟨110⟩ dumbbell interstitial defect that has the lowest energy.[1–3] The embedded atom method (EAM) potentials of Mendelev[4,5] have been directly fitted to this data and more recently also the magnetic potential (MP),[6,7] which explicitly takes into account the 0 K ferromagnetic aspect of bcc Fe. When using these potentials, defect statistics derived from multiple primary damage state cascade simulations appear to converge with respect to the total number of Frenkel Pairs produced.[8] However, some discrepancies still persist regarding the total number of clusters of point defects, indicating differences between the empirical potentials that cannot be controlled via knowledge of only the single interstitial defect energies. The static and dynamic properties of such complex defect structures are thus of increasing interest where detailed studies of vacancy and interstitial loop energetics and mobility,[9–11] as well as defect cluster interaction,[12] have been undertaken.

The vibrational properties of defects gives information about how a defect behaves at a finite temperature within a molecular-dynamics simulation and can be used to investigate the stability of defects through a comparison of the formation free energies. These vibrational properties are generally calculated within the harmonic approximation[13] to the crystal potential enabling a straightforward determination of thermodynamic quantities such as the vibrational free energy, entropy, and heat capacity. Moreover, through an analysis of the low-frequency modes, information can be gained at possible transition pathways for structural migration or transformation of defects. Work of this nature has been done to investigate the relative stability as a function of temperature of ⟨110⟩ and ⟨111⟩ single interstitials[14] as well as small clusters of interstitials forming either glissile prismatic loops[14] or so-called "self-trapped" sessile structures.[15] Work comparing the harmonic vibrational properties of vacancies with single interstitial and small interstitial loops for the above-mentioned empirical potentials has however revealed a wide spread in the defect formation entropies and therefore the temperature behavior of the corresponding formation free energies.[14] A recent *ab initio* calculation of the harmonic vibrational properties of the ⟨110⟩ and ⟨111⟩ dumbbell interstitials in bcc Fe (Ref. 16) now provides additional data through which a quantitative assessment of an empirical potential can be made.

It is however unclear to what extent the harmonic term contributes to the total free energy of the defect. For a perfect lattice containing inversion symmetry, third-order anharmonic contributions are expected to cancel at low temperatures and it is only at the fourth order that anharmonic contributions will begin to be present. At higher temperatures, where the atomic vibrations increasingly deviate away from the perfect lattice configuration, a non-negligble anharmonic contribution to the vibrational entropy and corresponding free energy will increasingly occur.[17] For the case of interstitials, which break the lattice symmetry at and around the core of the defect and also involve large local compressive

strains, little knowledge exists about the magnitude of the anharmonic contribution to the free energy. Additionally, the harmonic approach to estimating the free energy becomes problematic when defect diffusion occurs at a time scale comparable to the characteristic vibrational period of the defect. In this regime, where a diffusion event (a so-called lattice "hop") may no longer be considered a rare event, the defect cannot reach local thermal equilibrium before the next migration and the concept of a harmonic ground state becomes meaningless.

When this occurs, the usual transition state theory model of diffusion is no longer applicable and more general many-atom models that model the nonlinear dynamics of a defect must be considered such as the Frenkel-Kontorova model[18] which has been recently applied to understand the mobility of ⟨111⟩ crowdion single interstitial defects in nonmagnetic group 5B and 6B bcc transition metals.[19]

The main goal of this paper is to investigate the anharmonic contribution to the total formation free energy of the single ⟨110⟩ dumbbell interstitial by comparing the usual harmonic result with the anharmonic free energy obtained using a thermodynamic integration technique. This is done for the two well-known EAM Mendelev Fe potentials [Mendelev-2003 (Ref. 4) and Mendelev-2004 (Ref. 5)] and the published MP (MP-CS2) (Ref. 7), and also for two unpublished MPs (MP-CS3-00 and MP-CS3-30) that are additionally fitted to experimental low-temperature third-order elastic stiffness constants and are also able to reproduce correctly the nondegenerate core structure of the $\frac{1}{2}\langle 111\rangle$ perfect screw dislocation as do the Mendelev potentials but not the MP-CS2 potential. These new MPs arise from a considerable fitting effort in which an expanded materials database of both experimental and *ab initio* defect data has been exploited with the aim of producing a more accurate empirical potential for the radiation damage community. The Appendix contains their corresponding parametrization and a brief explanation of the MP, however, the full details of these potentials as well as the unique fitting strategy will be published separately.[20] These empirical potentials are included in the present work since by fitting to higher-order elastic constants, experimental anharmonic information is now included within their parametrization.

It is found that total formation entropies of the potentials presently considered fall within a bandwidth of $\sim 6k_B$, whereas the calculated harmonic formation free energies fall within a bandwidth of $\sim 30k_B$. It is seen that for the case of the Mendelev potentials and the newer MP fits, the harmonic approximation is able to estimate well the total free energy when calculating the vibrational free energy of the ⟨110⟩ dumbbell interstitial, particularly in the latter case where the new MPs are found to be strongly harmonic. In Sec. II, the harmonic and anharmonic computational methods are outlined and in Sec. III the harmonic and anharmonic free energies are presented and their temperature dependences rationalized via a study of the defect's corresponding vibrational formation entropy. In Sec. IV the results are discussed in terms of studying more complex defect structures and assessed in light of the fact that for bcc Fe at finite temperatures, magnetic fluctuations also contribute to the total free energy of the defect structure.

II. COMPUTATIONAL METHODS

A. Harmonic approximation to the free energy

The most popular method to calculate vibrational free energy of a particular atomic configuration is based on the harmonic approximation.[13] Within this approximation, the potential energy function $E(\vec{R}_1,\ldots,\vec{R}_N)$ of a periodic system of N atoms is expanded to the second order near a local minima obtained either by conjugate gradient or molecular statics structural relaxation methods. This local minimum defines the zero-temperature ground-state structure of the atomic configuration. Let the atomic coordinates of this local minima be given by $\vec{R}_1^0,\ldots,\vec{R}_N^0$ and let $\vec{u}_1,\ldots,\vec{u}_N$ be small displacements of the atoms away from this local minima. Then we have

$$E(\vec{R}_1^0+\vec{u}_1,\ldots,\vec{R}_N^0+\vec{u}_N) \approx E_{\text{local}} + \frac{1}{2}\sum_{\substack{i,j=1,\ldots,N \\ \mu,\nu=x,y,z}} u_i^\mu D_{ij}^{\mu\nu} u_j^\nu, \tag{1}$$

where $\mu,\nu=x,y,z$ refer to the Cartesian coordinate (polarization) directions, $i,j=1,\ldots,N$ are the atomic indices, and $E_{\text{local}}=E(\vec{R}_1^0,\ldots,\vec{R}_N^0)$ is the local energy minima. The translationally invariant force matrix is given by[21]

$$D_{ij}^{\mu\nu} = \Lambda_{ij}^{\mu\nu} - \delta_{ij}\sum_k \Lambda_{ik}^{\mu\nu}, \tag{2}$$

where $\hat{\Lambda}$ is the Hessian matrix of rank $3N$ defined by

$$\Lambda_{ij}^{\mu\nu} = \left.\frac{\partial^2 E(\vec{R}_1,\ldots,\vec{R}_N)}{\partial R_i^\mu\,\partial R_j^\nu}\right|_{\vec{R}_1^0,\ldots,\vec{R}_N^0}. \tag{3}$$

The classical vibrational free energy within the harmonic approximation is then given by[17]

$$F(T,N) = E_{\text{local}} + k_B T\sum_{n=1}^{3N-3} \ln\left(\frac{\hbar\omega_n}{k_B T}\right), \tag{4}$$

where $\omega_n=\sqrt{\frac{d_n}{M}}$, $n=1,\ldots,3N$ are the vibrational frequencies of the system calculated from the eigenvalues d_n of the force matrix $\hat{D}$. The sum in Eq. (4) excludes the zero-frequency translational modes and thus spans the positive $3N-3$ frequencies. Here M is the mass of an Fe atom, $\hbar$ is the Planck's constant, and k_B is the Boltzmann's constant.

The local atomic vibrational free energy is given by

$$F_i^\mu(T,N) = k_B T\sum_{n=1}^{3N-3} (U_{i,n}^\mu)^2 \ln\left(\frac{\hbar\omega_n}{k_B T}\right), \tag{5}$$

where $U_{i,n}^\mu$ is the projection onto atom i of the eigenvector associated with the nth eigenvalue along the direction μ, that is, $\hat{\Lambda}\tilde{U}_n=d_n\tilde{U}_n$. Note that due to the orthonormality of the eigenvectors $\tilde{U}_n$, $F(T,N)=E_{\text{local}}+\sum_{i\mu} F_i^\mu(T,N)$. The use of local atomic values of the vibrational free energy can give insight to the microscopic origin of the bulk value $F(T,N)$, particularly when defect structures are considered. It is however the

bulk value which is the physically meaningful quantity.

When considering either a perfect lattice or a defect structure, the corresponding atomic configuration is relaxed at a particular volume to obtain the force matrix. The chosen volume can be the 0 K equilibrium value or a value obtained from zero-pressure finite-temperature dynamical simulations. Performing a harmonic expansion at the chosen volume will result in the vibrational frequencies depending implicitly on that volume—this approach is referred to as the quasiharmonic approximation.[21,22] In what follows, the harmonic free energy will refer to a harmonic expansion at the 0 K equilibrium volume whose temperature dependence arises explicitly via Eq. (4). On the other hand, a quasiharmonic free energy at a given temperature T arises from a harmonic expansion at a volume obtained from zero-pressure dynamical simulations performed at temperature T where Eq. (4) is evaluated only at T.

B. Estimation of the anharmonic contribution to the free energy: The Frenkel-Ladd method

The free energy of a system is defined entirely by its Hamiltonian, $H_1=H_1[(\vec{r}_i,\vec{p}_i)]$ and cannot be expressed as a simple ensemble average such as can be done for internal energy, heat capacity, and stress. However by constructing the Hamiltonian

$$H(\lambda) = \lambda H_1 + (1-\lambda)H_0, \tag{6}$$

where $H_0=H_0[(\vec{r}_i,\vec{p}_i)]$ is a reference Hamiltonian, the difference in free energy can be expressed in terms of a thermodynamic integration over an ensemble average[23] with respect to $H(\lambda)$

$$F_1 - F_0 = \int_0^1 \frac{dF(\lambda)}{d\lambda} d\lambda = \int_0^1 \left\langle \frac{\partial H(\lambda)}{\partial \lambda} \right\rangle_\lambda d\lambda = \int_0^1 \langle H_1 - H_0 \rangle_\lambda d\lambda, \tag{7}$$

where

$$\langle H_1 - H_0 \rangle_\lambda = \frac{1}{Z_\lambda} \int d\vec{p}_1 \cdots d\vec{p}_N d\vec{r}_1 \cdots d\vec{r}_N (H_1 - H_0) \times \exp[-\beta H(\lambda)] \tag{8}$$

in which, Z_λ is the corresponding partition function of $H(\lambda)=\lambda H_1+(1-\lambda)H_0$, and $\beta=1/k_BT$.

Equation (4) can then be used to determine the total free energy F_1 of an N atom configuration by choosing a $H_0=H_0[(\vec{r}_i,\vec{p}_i)]$, for which F_0 is known, and calculating $\langle H_1-H_0\rangle_\lambda$ either via a molecular dynamics or an ensemble Monte Carlo (MC) simulation. In the present work we employ as a reference Hamiltonian, H_0; the harmonic expansion around a local minima [Eq. (1) in the previous section] and use the Monte Carlo numerical technique to determine the ensemble average. In this way, Monte Carlo simulations will yield F_1-F_0 via Eq. (7), which is the anharmonic contribution to the free energy. Adding the harmonic contribution [Eq. (4)] to this then gives the total free energy of the atomic system.

III. RESULTS

A. Formation free energy of the ⟨110⟩ interstitial dumbbell

The formation free energy of a point defect at temperature T is defined as

$$\Delta F(T) = F_{DB}(T,N+1) - \frac{N+1}{N} F_{\mathrm{bcc}}(T,N), \tag{9}$$

where $F_{DB}(T,N+1)$ and $F_{\mathrm{bcc}}(T,N)$ are, respectively, the absolute free energy of the periodic supercell containing $N+1$ atoms including the single interstitial and of the perfect bcc periodic supercell containing N atoms. The formation free energy may depend sensitively on whether the two supercells have the same volume, the same volume per atom, or the same pressure.

In the present section the free energy of the ⟨110⟩ dumbbell is calculated using the harmonic, the quasiharmonic, and the thermodynamic integration methods. For all cases a periodic simulation cell consisting of 2001 atoms for the interstitial configuration and 2000 atoms for the bcc reference lattice is employed to ensure minimal supercell size effects. For the harmonic calculation we relax the ⟨110⟩ dumbbell configuration using molecular statics in a simulation cell that has a fixed volume per atom equal to that of the 0 K equilibrium bcc volume per atom. For the quasiharmonic calculation, the ⟨110⟩ dumbbell is further relaxed at fixed volumes per atom corresponding to the 300, 400, 500, and 600 K equilibrium bcc volume per atom obtained from zero pressure molecular-dynamics simulations using the Parrinello-Rahman barostat method.[24] Table I shows the temperature-dependent equilibrium bcc cohesive energies and volumes for the empirical potentials used and we see that for the case of the MP-CS2 potential thermal contraction rather than thermal expansion occurs for the considered temperature range. Table I also displays the relaxed defect formation energies of the ⟨110⟩ dumbbell interstitial at these temperatures and corresponding fixed volumes per atom. For all empirical potentials a decrease in the relaxed formation energies occurs with decreasing temperature.

For the thermodynamic integration free-energy calculation, these fixed volumes per atom configurations are used in constant volume ensemble MC simulations at the corresponding temperatures to determine $\langle H_1-H_0\rangle_\lambda$ for $\lambda=0.00,0.05,0.1,\ldots,0.95,1.00$ using the Frenkel-Ladd method outlined in the previous section. To obtain a high level of precision the ensemble averages are performed using $\sim 10^8$ accepted Monte Carlo steps. Each trial Monte Carlo step involved a randomly chosen atom being randomly displaced by a maximum distance of 0.1 Å. We note that by keeping the volume fixed the present calculations do not consider free-energy contributions arising from volume fluctuations. Due to the translational invariance of the full Hamiltonian, $H_1=H_1[(\vec{r}_i,\vec{p}_i)]$, and therefore also of $H(\lambda)$ at $\lambda=1$, the center of mass of the system is also coupled to an artificial harmonic oscillator to minimize fluctuations in H_1-H_0 as λ approaches 1. The resulting free energies are then accordingly corrected using the known analytical result for the free energy of a harmonic oscillator to yield the total free energy of the defect.

TABLE I. Equilibrium bcc volume per atom (Å^3) and energy per atom (eV) as a function of temperature for the empirical potentials considered in the present work. Also shown are the ⟨110⟩ interstitial dumbbell formation energies (eV) as a function of temperature for atomic configurations whose volume per atom is set to the corresponding equilibrium bcc volume per atom.

Temperature (K)	bcc equilibrium volume per atom (Å^3)	bcc energy per atom (eV)	⟨110⟩ dumbbell formation energy (eV)
	MP-CS2		
0	11.7768	−4.3160000	3.65
300	11.7381	−4.3159312	3.63
400	11.7135	−4.3158156	3.61
500	11.6972	−4.3157079	3.60
600	11.6912	−4.3156619	3.60
	Mendelev-2003		
0	11.6393	−4.12243923	3.52
300	11.6845	−4.12234347	3.51
400	11.7141	−4.12217542	3.51
500	11.7472	−4.12189093	3.50
600	11.7859	−4.12142889	3.49
	Mendelev-2004		
0	11.6393	−4.01298646	3.53
300	11.7001	−4.01280968	3.51
400	11.7295	−4.01259930	3.51
500	11.7602	−4.01229416	3.50
600	11.7948	−4.01186661	3.49
	MP-CS3-00		
0	11.7768	−11.64735826	4.19
300	11.9001	−11.64683629	4.13
400	11.9297	−11.64650881	4.12
500	11.9595	−11.64610405	4.11
600	11.9889	−11.64562897	4.09
	MP-CS3-30		
0	11.7768	−9.89319216	4.23
300	11.8387	−9.89301704	4.21
400	11.8573	−9.89289711	4.20
500	11.8755	−9.89274959	4.19
600	11.8941	−9.89256858	4.18

Figure 1 displays $\langle H_1 - H_0 \rangle_\lambda$ for the interstitial defect, as a function of λ for the temperatures 300 and 600 K. Data for all potentials are shown. Each data point represents the average of approximately 300 000–500 000 accepted Monte Carlo steps. For the 300 K calculation good convergence is seen for all values of λ and the thermodynamic integration may be easily performed. On the other hand, for the 600 K calculation, $\langle H_1 - H_0 \rangle_\lambda$ does not converge for λ values at and close to unity indicating large fluctuations in $H_1 - H_0$ occur during the MC sampling. The origin of such fluctuations lies in the interstitial defect undergoing diffusion, where inspection of the 600 K atomic configurations derived from the Monte Carlo simulations reveals that the ⟨110⟩ dumbbell has moved to a rotated ⟨110⟩ dumbbell centered at a different site which is consistent with the diffusion mechanism of the nudged elastic band calculation of Fig. 2. This occurs naturally in the full Hamiltonian of the system $H_1 = H_1[(\vec{r}_i, \vec{p}_i)]$ while being entirely suppressed in the reference (harmonic) Hamiltonian $H_0 = H_0[(\vec{r}_i, \vec{p}_i)]$. At values of λ close to unity, diffusion is therefore allowed resulting in large values of H_0 since the defect is far away from the Harmonic minimum. This is a fundamental limitation of the Frenkel-Ladd method.

Although diffusion is present in the 600 K simulations, the ⟨110⟩ dumbbell interstitial defect will spend most of its time in its ground-state configuration and the lack of convergence encountered in Fig. 1 can be remedied by standard cubic-spline extrapolation of $\langle H_1 - H_0 \rangle_\lambda$ to values of λ near 1. That diffusion occurs at 600 K is confirmed in Fig. 2, which displays the minimum-energy migration pathway obtained via a nudged elastic band calculation[25] for the ⟨110⟩ dumbbell interstitial to "hop" a nearest-neighbor (NN) distance for all potentials. We see that the barrier heights of the considered potentials range from 0.25 to 0.4 eV—a migration energy barrier scale that will easily facilitate diffusion within the sampling size of the MC procedure used presently. The consequences of this and more generally of diffusion are very important when considering the free energy of a defect and will be discussed in more details in Sec. III.

Figure 3 displays the harmonic, quasiharmonic, and total formation free energies as a function of temperature for the potentials considered. There are significant differences across the empirical potentials due first to the different zero-temperature formation energies (see Table I) and second to the different temperature dependencies of the free energy. The latter being particularly the case for MP-CS2 [Fig. 3(b)], where the harmonic and quasiharmonic formation free energies increase with increasing temperature. When comparing the harmonic, quasiharmonic, and total formation free energies for a given potential, we see that the harmonic values generally overestimate the free energy. For the MP-CS2 potential [Fig. 3(b)], the over estimation is considerable indicating its strongly anharmonic nature, whereas for the Mendelev [Fig. 3(a)] and MP-CS3 [Fig. 3(c)] potentials the anharmonic correction is relatively small and indeed negligible for the MP-CS3-30 potential.

B. Formation entropies

The temperature dependence of the vibrational free energy may be largely understood from knowledge of the vibrational entropy. Thermodynamically, entropy may be obtained from the free energy via

$$S = -\frac{\partial F}{\partial T}. \tag{10}$$

For a direct measure of the total formation entropy, the results contained within Fig. 3 are fitted to $\Delta F(T) = \Delta E_0 - \Delta S_V T$, where ΔE_0 is the 0 K formation energy of the ⟨110⟩

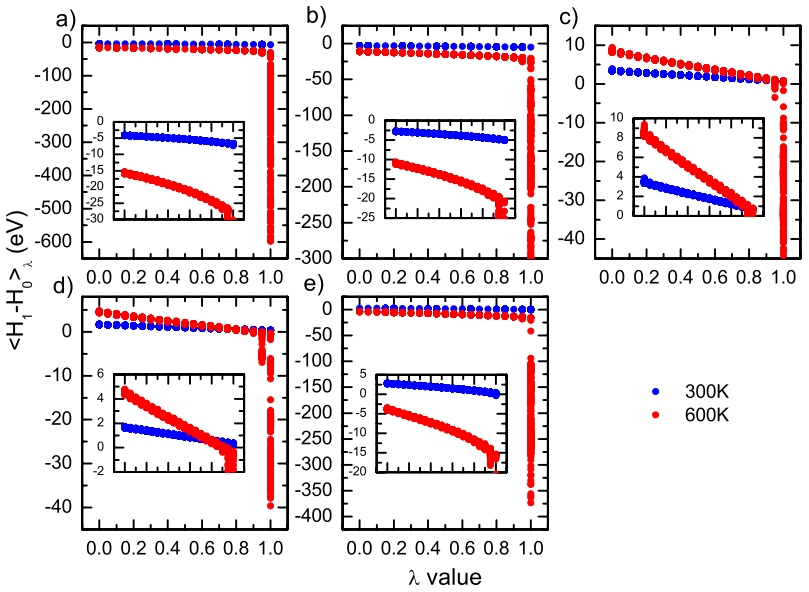

FIG. 1. (Color online) $\langle H_1 - H_0 \rangle_\lambda$ for the ⟨110⟩ interstitial dumbbell as a function of the thermodynamic integration parameter λ for the temperatures 300 and 600 K for the empirical potentials (a) Mendelev-2003, (b) Mendelev-2004, (c) MP-CS3-00, (d) MP-CS3-30, and (e) MP-CS2. At values of λ close to unity, $\langle H_1 - H_0 \rangle_\lambda$ does not converge for all empirical potentials due to diffusion of the defect.

dumbbell taken from Table I and ΔS_V is the formation entropy at fixed volume per atom. We note that the formation entropy of a defect structure is defined analogously to the formation free energy [Eq. (9)]. In columns one to four of Table II we show the results of this method applied to all three free-energy estimates. While absolute entropy can only be positive, the formation entropy of a defect can be negative and can simply indicate that the defect lowers the entropy relative to that of the surrounding lattice.

Within the harmonic and quasiharmonic approximations, the absolute global and local vibrational entropies may be easily obtained by explicitly differentiating Eqs. (4) and (5), respectively. Table II also lists for all potentials of the harmonic formation entropy at 300 K at fixed volume (ΔS_0), constant volume per atom (ΔS_V), and zero hydrostatic pressure (ΔS_P). For the case of fixed volume and constant volume interstitial structures, the reference is the equilibrium bcc lattice for the corresponding potential. Data from the literature are also shown, in particular, the constant pressure calculation of Marinica and Willaime[14] and a recent *ab initio* calculation of Lucas and Schaeublin.[16] Figure 4 displays these results as a function of volume per atom. For the Mendelev-2003 and MP-CS2 potentials, the formation entropy decreases with increasing volume per atom, while for the Mendelev-2004 and MP-CS3 potentials the formation entropy increases. These values compare favorably to the harmonic values derived from the fit to $\Delta F(T) = \Delta E_0 - \Delta S_V T$ also shown in Table II.

The trends seen in Fig. 4 as a function of volume can be largely understood by assuming that the difference between ΔS_V and ΔS_P arises from how the surrounding bcc lattice responds to the change in volume per atom. For an undistorted bcc lattice it can be shown that the change in entropy is given by

$$\Delta S = S_V - S_P = \alpha B \Delta V, \tag{11}$$

where α is the constant pressure thermal volume expansion coefficient, B is the isobaric bulk modulus, and ΔV is the corresponding change in volume. Assuming this expression, Fig. 5(a) plots the derived thermal volume expansion coefficients for the potentials. Thus the anomalous volume per atom dependence seen for the Mendelev-2003 and MP-CS2 potentials may be understood through these potentials exhibiting a negative thermal expansion at $T=0$. To assess the validity of Eq. (11), finite temperature and zero-hydrostatic pressure molecular dynamics simulations using the Parrinello-Rahman barostat method[24] are performed for the bcc lattice as a function of low temperature and the mean volume per atom measured. Figure 5(b) plots this as a function of temperature for all the potentials and we see again (see Table I) that the MP-CS2 potential exhibits thermal contraction with increasing temperature. For the Mendelev-2003 potential thermal contraction is also evident at these low temperatures with thermal expansion beginning at approximately 50 K. For the remaining potentials a positive thermal-expansion coefficient is found—indeed in Ref. 5 it is stated that the Mendelev-2004 has been corrected to produce a positive thermal expansion. The corresponding zero-pressure thermal-expansion coefficients are obtained by taking the

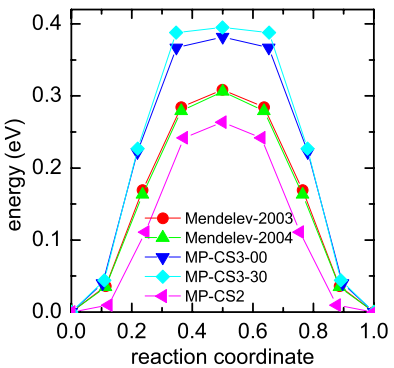

FIG. 2. (Color online) The migration pathways of a ⟨110⟩ dumbbell interstitial derived from a nudged elastic band calculation for the empirical potentials Mendelev-2003, Mendelev-2004, MP-CS3-00, MP-CS3-30, and MP-CS2.

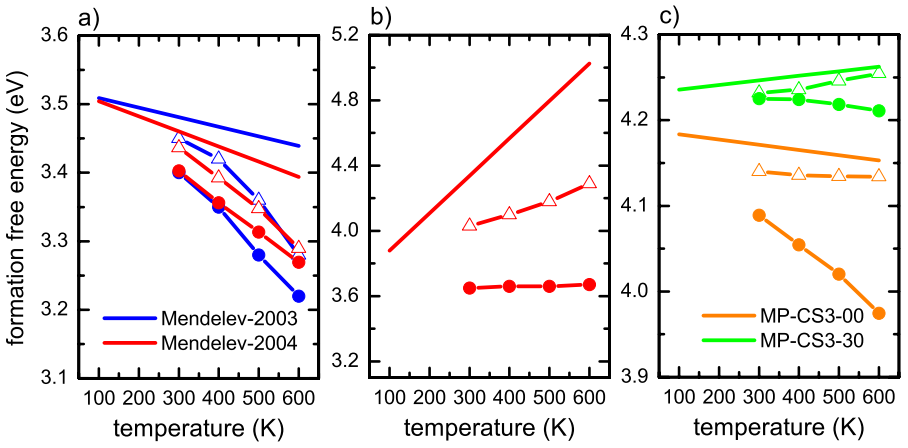

FIG. 3. (Color online) The formation free energy of the ⟨110⟩ dumbbell interstitial derived from the harmonic, quasiharmonic, and thermodynamic integration techniques using (a) the Mendelev-2003 and Mendelev-2004 empirical potentials, (b) the MP-CS2 empirical potential, and (c) the MP-CS3-00 and MP-CS3-30 empirical potentials. The solid lines represent the harmonic, the triangled data represent the quasiharmonic, and the filled circles represent the total free energy.

gradient of these curves at $T=0$ and are displayed in Fig. 5(a) demonstrating good agreement with those calculated through Eq. (11). Thus the volume dependence of the formation entropies is primarily due to the entropy change in the surrounding lattice, which can be reasonably well described by the thermal-expansion properties of the corresponding empirical potential via Eq. (11). On the other hand, as shall be demonstrated in the following paragraphs, the absolute value of the formation entropy appears to be more strongly controlled by the core properties of the interstitial which in turn depends sensitively on the shorter range (far from equilibrium) properties of the empirical potential.

Figure 6 displays a 110 plane of atoms containing the interstitial defect in the center. Also shown are four off-plane atoms which are nearest neighbor to the two atoms of the split dumbbell–for location of the interstitial dumbbell and these off-plane atoms see the inset in Fig. 6(a). The simulation cell has a volume per atom equal to that of the corresponding 0 K bcc lattice. Figures 6(a) and 6(b) are for the MP-CS2 potential, Figs. 6(c) and 6(d) are for the Mendelev-2003 potential and Figs. 6(e) and 6(f) are for the MP-CS3-30 potential. In Figs. 6(a), 6(c), and 6(e) the atoms are colored according to their hydrostatic pressure calculated using the virial expression[26] and we see that the local pressure signature of the interstitial is similar for all three potentials. We note that in all cases the atoms far from the interstitial core are close to zero pressure. This is typical when using atomic configurations that have a fixed volume per atom equal to that of the bulk. Figures 6(b), 6(d), and 6(f) show the same atoms now colored according to their local harmonic entropies relative to the equilibrium bulk bcc in units of the Boltzmann constant calculated at 300 K. Unlike the pressure distribution, large differences in the local entropy signatures are seen at the core of the defect across all three potentials. We note that in Figs. 6(b), 6(d), and 6(f) those atoms having entropy less than $-0.2k_B$ are all similarly colored dark blue and those having a value greater than $0.2k_B$ are similarly colored red. For intermediate values the corresponding linear color bar can be used. For the MP-CS2 potential the core atoms all have local relative entropies that are less than that of the perfect lattice with the split dumbbell atoms having the most negative value of $-1.2k_B$. On the other hand for the Mendelev-2003 potential the core atoms are generally greater than the perfect lattice varying between $-0.066k_B$ and $0.28k_B$ for the split dumbbell atoms. For the MP-CS3-30 potential the variation in local entropies relative to the perfect lattice is somewhat intermediate varying between $-0.188k_B$ and $0.099k_B$. We note that the local entropy signature for the Mendelev-2004 potential (not shown) is quite similar to that of the Mendelev-2003 potential, whereas for the MP-CS3-00 potential (not shown), the entropy signature differs at the core region from that of MP-CS3-30 by several k_B.

Figure 7 shows only the core interstitial atoms using the same viewing direction as in Fig. 6, where now the atoms are colored according to their fractional local entropies in which

TABLE II. Formation entropies in units of k_B of the ⟨110⟩ interstitial dumbbell obtained by linear fitting to the free-energy curves of Fig. 3 and also via explicit calculation through Eqs. (4) and (9). For comparison, values are also shown from a similar calculation (Ref. 14) using the considered empirical potential (in parenthesis) and an *ab initio* result (Ref. 16).

	Harmonic method	Quasiharmonic method	Thermodynamic integration method	Harmonic ΔS_0	Harmonic ΔS_V	Harmonic ΔS_P
MP-CS2	−26.58	−12.71	−0.28	−23.66	−26.59	−24.73
Mendelev-2003	1.80	4.08	5.67	2.94	1.62	1.27 (2.84)
Mendelev-2004	2.55	4.20	4.92	1.81	2.72	4.02
MP-CS3-00	0.71	1.31	4.02	−5.39	0.53	3.13
MP-CS3-30	−0.63	−0.34	0.28	−4.17	−0.65	0.69
Ab initio (Ref. 16)					0.24	

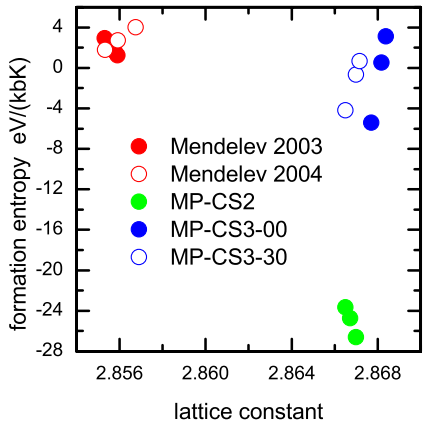

FIG. 4. (Color online) Harmonic formation entropies of the ⟨110⟩ dumbbell interstitial as a function of lattice constant for the considered empirical potentials at 500 K.

zero represents the minimum value and unity the maximum value of the core structure for the given potential. For the case of MP-CS2 [Fig. 7(a)] the two split dumbbell core atoms have the minimum (most negative at $-1.2k_B$) local relative entropy with the neighboring atom's entropies increasing to the maximum value. For MP-CS3-30 [Fig. 7(c)] a larger number of core atoms have a local entropy near the minimum value (most negative at $-0.188k_B$). On the other hand for the Mendelev-2003 potential [Fig. 7(b)] the split dumbbell pair of atoms has the maximum local entropy at $0.28k_B$. Thus in terms of the local entropy signature the three investigated potentials give widely different signatures corresponding to differing total formation entropies (Fig. 4) and thus differing temperature-dependent formation free energies.

IV. DISCUSSION AND CONCLUDING REMARKS

When considering the applicability of the presented free-energy calculations a number of factors must be considered that are specific to bcc Fe. In particular, ferromagnetism stabilizes the Fe bcc phase at low temperatures and with rising temperature, spin fluctuations play an increasingly important role in material bonding leading to the α-bcc to γ-fcc phase transition at ~1000 K.[27] Such magnetic spin fluctuations will contribute in two ways that have not been included in the current calculation. First, spin fluctuations will directly affect the interatomic bonding giving an explicit and strong temperature dependence of related material properties.[28,29] For example, the elastic stiffness constants of bcc Fe are known to change significantly as the temperature approaches the Curie temperature,[30,31] resulting in a strong increase in the elastic anisotropy due to the ⟨110⟩ shear modulus decreasing finally to zero at the α-bcc to γ-fcc phase transition. Recently this aspect has been used to explain the energetics of ⟨100⟩ and ⟨111⟩ prismatic dislocation loops in bcc Fe as a function of temperature,[32] where the anisotropic elastic energy of the former scales as a square root of the 110 shear modulus. It is therefore expected that such a change in the ⟨110⟩ shear modulus will also strongly affect the elastic field around the ⟨110⟩ dumbbell interstitial leading to a non-negligible temperature dependence of the defect's formation energy. Inspection of the temperature dependence of the elastic stiffness constants reveals significant changes that have already occurred at approximately 600–700 K,[31] and since current empirical potentials are all fitted to either 0 K or low temperature experimental elastic constants this sets an upper temperature limit to the applicability of the present results. We note that this limitation does not only apply to the present calculations but *all* atomistic calculations that employ empirical potentials to study the high-temperature behavior of defect structures within bcc Fe. A second aspect is the entropic contribution due to the additional degrees of freedom associated with the spin fluctuations, which must also be added to the free energy. The recent development of a spin lattice dynamics simulation technique for bcc Fe that converges to the MP formalism at 0 K (Ref. 33) offers a promising method to address this aspect and to ascertain the quantitative contribution of spin fluctuations to the formation entropy and free energy of a defect.

As with all such classical molecular dynamics or Monte Carlo simulations there also exists a lower temperature range below which quantum effects begin to dominate. A general rule is that such simulations should not be performed at temperatures approximately one third below the Debye tempera-

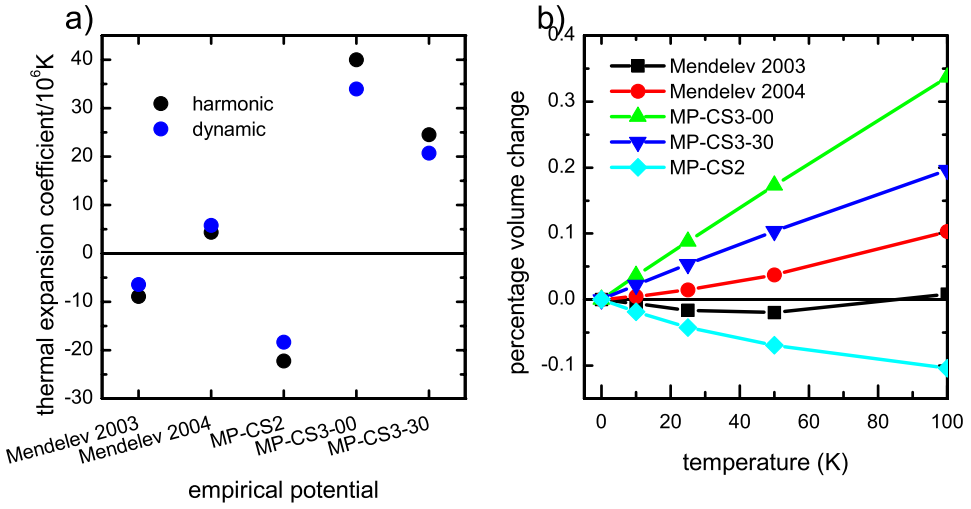

FIG. 5. (Color online) (a) Thermal-expansion coefficients derived from formation entropy volume dependence and finite-temperature molecular dynamics simulations and (b) percentage volume increase as a function of temperature derived from molecular dynamics calculations.

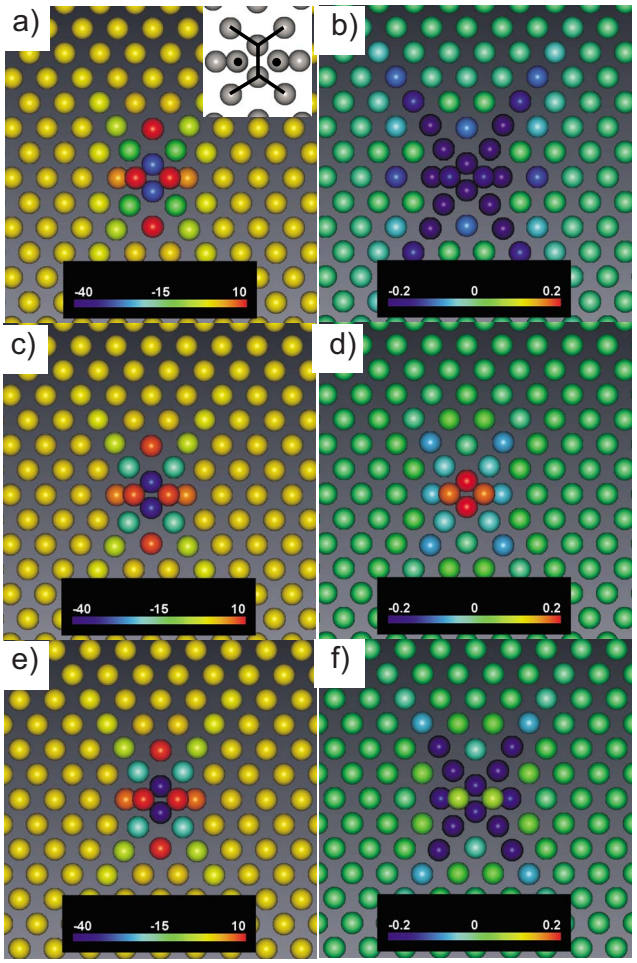

FIG. 6. (Color online) Atomic 110 plane containing a ⟨110⟩ dumbbell interstitial defect where in (a), (c), and (e) atoms are colored according to their local hydrostatic pressure and in (b), (d), and (f) atoms are colored according to their local harmonic vibrational entropies at 500 K. (a) and (b) are for the MP-CS2 potential, (c) and (d) are for the Mendelev-2003 potential, and (e) and (f) are for the MP-CS3-30 potential. Inset in Fig. 6(a) is a schematic of the dumbbell with the same orientation of that of the main figure with the 110 dumbbell axis pointing upwards. Those atoms labeled with a black circle are above the 110 atomic plane and are NN to the split dumbbell.

ture of the material; a regime where the Bose-Einstein distribution of phonon energies begin to strongly manifest itself. For bcc Fe the Debye temperature is ~470 K and thus classical molecular dynamical simulations should not be performed at temperatures lower than ~150 K. Such quantum effects can be addressed within the harmonic approximation by replacing the Maxwell-Boltzmann distribution used in Eqs. (4) and (5) with the Bose-Einstein distribution; however for dynamical calculations, no computationally efficient method suitable for large atomic configurations is available.

Thus if one does not consider the entropy due to spin fluctuations, the applicable range of the present free-energy calculations is between ~150 and ~700 K, which is at the lower temperature end of the range of temperatures where ferritic and ferritic martensitic steels are expected to be used in fission and fusion applications.

The total free-energy calculations also reveal the onset of diffusion at temperatures above ~500 K. Diffusion of the ⟨110⟩ dumbbell interstitial at these higher temperatures remains a rare event, in the sense that the defect has time to equilibrate before its next lattice "hop," and thus it becomes valid to decouple entropy contributions into a vibrational term and a lattice configuration term as has been done here and in previous works. Such a separation is however not justified for the higher energy ⟨111⟩ interstitial defect structure which is inherently unstable in bcc Fe for all temperatures. Moreover in nonmagnetic bcc transition metals, where it is the ⟨111⟩ interstitial defect that is the lowest energy structure, the defect is inherently mobile at all temperatures with a migration barrier in the sub 100 meV energy range.[3,19,34,35] Thus diffusion cannot be considered as a sequence of rare events and the 0 K relaxed structure and its vibrational frequency spectrum will give little insight into the thermal excitations of the mobile defect. It is for these reasons that the present work does not consider the harmonic properties of the ⟨111⟩ interstitial, despite the harmonic approximation being adequate for the ⟨110⟩ interstitial for some empirical potentials. Past work that compares the harmonic free energies of the ⟨110⟩ and ⟨111⟩ defects as a function of temperature in Fe, and in particular, a crossover of stability at higher temperatures, should therefore be treated with care.

The present work has been performed using five modern empirical potentials which demonstrate quite different defect entropy core signatures with the greatest difference originating from the MP-CS2 potential. Although it is difficult to rationalize the present results in terms of general features of these empirical potentials, recent work[20] has shown that the MP-CS2 potential is wrongly and strongly anharmonic as evidenced in Fig. 3(b). It was found that the third-order elastic constants of MP-CS2 are large and in some cases of the incorrect sign when compared to experiment. For the Mendelev-2003, Mendelev-2004, and MP-CS3 potentials, a

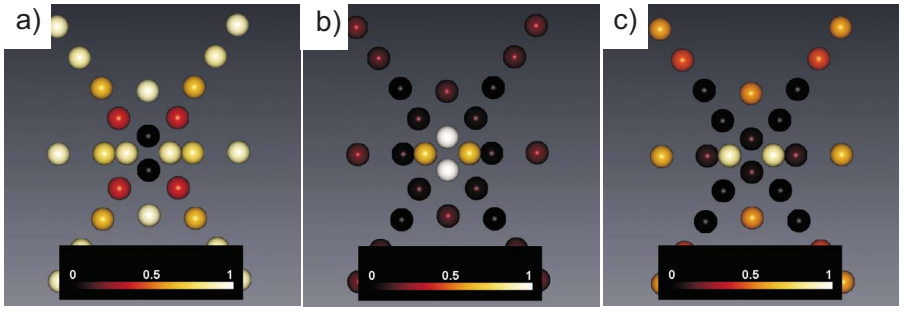

FIG. 7. (Color online) Core atoms of ⟨110⟩ dumbbell visualized for the (a) MP-CS2, (b) Mendelev-2003, and (c) MP-CS3-30 potentials. Atoms are colored according to their fractional local entropies derived from each of the minimum and maximum entropy values of the corresponding core configuration.

TABLE III. Optimal parameter set for MP-CS3-00 and MP-CS3-30.

	MP-CS3-00		MP-CS3-30	
A	18.42439658215181		14.96128089567820	
B	6.318801651265125		4.754553632722176	
Knot point	f_n	r_n^f	f_n	r_n^f
1	1.415806965777580	3.600000000000000	2.403773687542704	3.600000000000000
2	−3.172941853042061	3.457142857142857	−5.616539002612204	3.457142857142857
3	2.518779011423245	3.314285714285715	4.518414772417062	3.314285714285715
4	1.5223391656998341E-002	3.171428571428572	0.4511822086528371	3.171428571428572
5	−2.668402591084014	3.028571428571428	−3.719791696378764	3.028571428571428
6	5.300933735220243	2.885714285714286	3.176870270223375	2.885714285714286
7	−6.253127207203284	2.742857142857143	−0.5435529434135428	2.742857142857143
8	4.354340872738243	2.600000000000000	4.835150824080221	2.600000000000000
Knot point	V_n	r_n^V	V_n	r_n^V
1	0.1671995832644735	3.640000000000000	4.852979304356857	3.400000000000000
2	5.748723734256789	3.457142857142857	−7.762255546111966	3.285714285714286
3	1.238260767101568	3.285714285714286	0.2118336138629596	3.171428571428571
4	−27.80866986307653	3.114285714285714	−1.592481362817459	3.057142857142857
5	47.11807523555423	2.942857142857143	0.1193277971484847	2.942857142857143
6	−27.30051838220325	2.771428571428571	23.52407656927417	2.828571428571429
7	−0.1513119116248357	2.600000000000000	−7.298957800246290	2.714285714285714
8	40.00000000000000	2.500000000000000	−1.386774762653686	2.600000000000000
λ_f	1.67606860		2.04390805	
λ_V	1.54501120		0.19900397	

similar analysis has demonstrated the third-order elastic constants to be smaller and generally of the correct sign. This is a somewhat reasonable conclusion since how the lattice immediately surrounding the defect deforms (nonlinearly) will be controlled by such higher-order moduli. This aspect should be considered when developing new semiempirical potentials.

In conclusion, the harmonic and anharmonic contributions to the free energy of the ⟨110⟩ interstitial dumbbell have been calculated using the thermodynamic integration method. The present work shows for the Mendelev potentials[4,5] and a class of developed magnetic potentials[20] fitted to the third-order elastic stiffness constants that the harmonic approximation to the free energy works relatively well since these potentials are not strongly anharmonic. This is an encouraging result since it justifies, when diffusion is absent or minimal, the often used harmonic approximation approach of diagonalizing the force matrix of a relaxed defect structure to obtain its vibrational properties. In fact the harmonic approximation to the vibrational free energy and entropy can be routinely used for large defect structures such as interstitial clusters, dislocations, dislocation loops, and grain boundaries, whereas the thermodynamic integration calculation of the free energy and entropy is a computationally intensive procedure restricted to temperatures above the Debye value, where the classical Maxwell-Boltzmann distribution of vibrational excitations is justified. It however must be remembered that, unique to bcc Fe, there also exists a contribution to the free energy due to the degrees of freedom associated with spin fluctuations at finite temperature and that these must also be taken into account when conclusions are made about defect structure stability—particularly at the higher temperature range.

ACKNOWLEDGMENTS

S.C. and P.M.D. acknowledge the Paul Scherrer Institut–Forschungskommission for partial financial support and Helena Van Swygenhoven for her support of this project. This work was also partly funded jointly by the United Kingdom Engineering and Physical Sciences Research Council and by the European Communities under the contract of Association between EURATOM and UKAEA. This work was carried out within the framework of the European Fusion Development Agreement.

APPENDIX: THE MAGNETIC POTENTIAL

The magnetic potential[6,7] is an interatomic potential for bcc Fe based on the Stoner model of ferromagnetism within the second-moment approximation to the electronic density of states. The energy for a given configuration of N atoms is of the EAM form

$$E = \sum_{i=1}^{N} F[\rho_i] + \frac{1}{2}\sum_{i\neq j}^{N} V(r_{ij}), \tag{A1}$$

where $V(r)$ is a repulsive pair potential and

$$\rho_i = \sum_{i\neq j}^{N} f(r_{ij}) \tag{A2}$$

is the local electronic density on atom i. In Eq. (A1), the embedding energy is given by

$$F[\rho] = -A\sqrt{\rho} - \frac{B}{\ln 2}(1-\sqrt{\rho})\ln(2-\rho)\Theta(1-\rho). \tag{A3}$$

Here the first term represents the regular Finnis-Sinclair[36] nonmagnetic d-state band energy and the second term the ferromagnetic band energy where $\Theta(x)$ is the Heaviside step function which switches off ferromagnetism when $\rho > 1$. The original parametrization (MP-CS2) is given in Ref. 7 in which the radial functions are represented via third-order knot functions.

The parametrizations MP-CS3-00 and MP-CS3-30 used in the present work constitute the partial results of a fitting attempt[20] of the MP formalism [Eqs. (A1)–(A3)] to a wider range of bcc Fe experimental and *ab initio* data including third-order elastic constants, the nondegenerate core structure of a $\frac{1}{2}\langle 111\rangle$ perfect screw dislocation via the fitting to a multistring Frenkel-Kontrova model of the screw dislocation.[37] To include continuity of the radial functions to the fourth derivative the radial functions $V(r)$ and $f(r)$ are represented by fifth-order knot functions modulated by an exponential

$$V(r) = \sum_{n=1}^{N^V} V_n (r_n^V - r)^5 e^{-\lambda_V (r_n^V - r)} \Theta(r_n^V - r), \tag{A4}$$

$$f(r) = \sum_{n=1}^{N^f} f_n (r_n^f - r)^5 e^{-\lambda_f (r_n^f - r)} \Theta(r_n^f - r). \tag{A5}$$

Here the positions of the knot functions r_n^V and r_n^f, their coefficients V_n and f_n, and λ_V and λ_f values become fitting parameters of the optimization. For completeness of the present work we present the parametrizations for MP-CS3-00 and MP-CS3-30 in Table III. The bulk equilibrium properties to which these potentials have been fitted to are contained in Ref. 7–importantly, the equilibrium bcc lattice constant for MP-CS3-00 is 2.867 696 Å and for MP-CS3-30 it is 2.8665 Å. The broad fitting approach and the specific defect database of material properties and how they have been weighted during the fit will be presented in Ref. 20.

[1] C. Domain and C. S. Becquart, Phys. Rev. B **65**, 024103 (2001).
[2] C. C. Fu, F. Willaime, and P. Ordejon, Phys. Rev. Lett. **92**, 175503 (2004).
[3] D. Nguyen-Manh, A. P. Horsfield, and S. L. Dudarev, Phys. Rev. B **73**, 020101 (2006).
[4] M. I. Mendelev, S. Han, D. J. Srolovitz, G. J. Ackland, D. Y. Sun, and M. Asta, Philos. Mag. **83**, 3977 (2003).
[5] G. J. Ackland, M. I. Mendelev, D. J. Srolovitz, S. Han, and A. V. Barashev, J. Phys.: Condens. Matter **16**, S2629 (2004).
[6] P. M. Derlet and S. L. Dudarev, Prog. Mater. Sci. **52**, 299 (2007).
[7] S. L. Dudarev and P. M. Derlet, J. Phys.: Condens. Matter **17**, 7097 (2005).
[8] C. Bjorkas and K. Nordlund, Nucl. Instrum. Methods Phys. Res. B **259**, 853 (2007).
[9] M. A. Puigvi, Y. N. Osetsky, and A. Serra, Philos. Mag. **83**, 857 (2003).
[10] Y. N. Osetsky, A. Serra, B. N. Singh, and S. I. Golubov, Philos. Mag. A **80**, 2131 (2000).
[11] M. R. Gilbert, S. L. Dudarev, P. M. Derlet, and D. G. Pettifor, J. Phys.: Condens. Matter **20**, 345214 (2008).
[12] J. Marian, B. D. Wirth, and J. M. Perlado, Phys. Rev. Lett. **88**, 255507 (2002).
[13] A. A. Maradudin, E. W. Montroll, G. H. Weiss, and I. P. Ipatova, *Theory of Lattice Dynamics in the Harmonic Approximation* (Academic, New York, 1971).
[14] M. C. Marinica and F. Willaime, Solid State Phenom. **129**, 67 (2007).
[15] D. A. Terentyev, T. P. C. Klaver, P. Olsson, M. C. Marinica, F. Willaime, C. Domain, and L. Malerba, Phys. Rev. Lett. **100**, 145503 (2008).
[16] G. Lucas and R. Schaeublin (unpublished).
[17] S. M. Foiles, Phys. Rev. B **49**, 14930 (1994).
[18] O. M. Braun and K. S. Kivshar, *The Frenkel-Kontorova Model* (Springer, New York, 2004).
[19] S. P. Fitzgerald and D. Nguyen-Manh, Phys. Rev. Lett. **101**, 115504 (2008).
[20] S. Chiesa, P. M. Derlet, S. L. Dudarev, and H. Van Swygenhoven (unpublished).
[21] N. W. Ashcroft and N. D. Mermin, *Solid State Physics* (Holt, Rinehart, and Winston, New York, 1976).
[22] M. T. Dove, *Structure and Dynamics: An Atomic View of Materials* (Oxford University Press, Oxford, 2003).
[23] D. Frenkel and A. J. C. Ladd, J. Chem. Phys. **81**, 3188 (1984).
[24] M. Parrinello and A. Rahman, J. Appl. Phys. **52**, 7182 (1981).
[25] G. Henkelman, G. Johannesson, and H. Jonsson, in *Progress on Theoretical Chemistry and Physics*, edited by S. D. Schwartz (Kluwer Academic, Dordrecht, 2000).
[26] D. Frenkel and B. Smit, *Understanding molecular simulation* (Academic, New York, 2002).
[27] H. Hasegawa and D. G. Pettifor, Phys. Rev. Lett. **50**, 130 (1983).
[28] S. L. Dudarev and P. M. Derlet, J. Comput. Aided Mater. Des. **14**, 129 (2007).
[29] S. L. Dudarev, P. M. Derlet, and R. Bullough, J. Nucl. Mater. **386-388**, 45 (2009).
[30] D. J. Dever, J. Appl. Phys. **43**, 3293 (1972).

[31] S. K. Satija, R. P. Comes, and G. Shirane, Phys. Rev. B **32**, 3309 (1985).
[32] S. L. Dudarev, R. Bullough, and P. M. Derlet, Phys. Rev. Lett. **100**, 135503 (2008).
[33] P. W. Ma, C. H. Woo, and S. L. Dudarev, Phys. Rev. B **78**, 024434 (2008).
[34] P. M. Derlet, D. Nguyen-Manh, and S. L. Dudarev, Phys. Rev. B **76**, 054107 (2007).
[35] D. Nguyen-Manh, S. L. Dudarev, and A. P. Horsfield, J. Nucl. Mater. **367-370**, 257 (2007).
[36] M. W. Finnis and J. E. Sinclair, Philos. Mag. A **50**, 45 (1984).
[37] M. R. Gilbert and S. L. Dudarev, Philos. Mag. (to be published).